KEK Report 86- 6
November 1986
M

PHOTOIONIZATION OF SUBVALENCE P-SUBSHELL IN ALKALI AND ALKALINE-EARTH ATOMS

A. YAGISHITA, T. HAYAISHI, Y. ITOH, T. KOIZUMI, T. MATSUO, J. MURAKAMI,
T. NAGATA, Y. SATO, H. SHIBATA, M. YOSHINO and Y. ITIKAWA

NATIONAL LABORATORY FOR
HIGH ENERGY PHYSICS

KEK Reports are available from:

Technical Information Office
National Laboratory for High Energy Physics
Oho-machi, Tsukuba-gun
Ibaraki-ken, 305
JAPAN

Phone: 0298-64-1171
Telex: 3652-534 (Domestic)
(0)3652-534 (International)
Cable: KEKOHO

Photoionization of Subvalence p-subshell in Alkali and Alkaline-earth Atoms

A. Yagishita, T. Hayaishi[1], Y. Itoh[2], T. Koizumi[3], T. Matsuo[4], J. Murakami[5], T. Nagata[6], Y. Sato[5], H. Shibata[7], M. Yoshino[8] and Y. Itikawa[9]

Photon Factory, National Laboratory for High Energy Physics,
Oho-machi, Tsukuba-gun, Ibaraki 305, Japan

(Footnotes)

1. Permanent address: Institute of Applied Physics, University of Tsukuba, Sakura-mura, Niihari-gun, Ibaraki 305, Japan
2. Permanent address: Faculty of Science, Josai University, Keyakidai, Sakado-shi, Saitama 350-02, Japan
3. Permanent address: Department of Physics, Rikkyo University, Nishi-Ikebukuro, Toshima-ku, Tokyo 171, Japan
4. Permanent address: Medical Research Institute, Tokyo Medical and Dental University, Yushima, Bunkyo-ku, Tokyo 113, Japan
5. Permanent address: Research Institute for Scientific Measurements, Tohoku University, Katahira, Sendai-shi, Miyagi 980, Japan
6. Permanent address: Department of Science and Technology, Meisei University, Hodokubo, Hino-shi, Tokyo 191, Japan
7. Permanent address: Research Center for Nuclear Science and Technology, The University of Tokyo, Tokai-mura, Naka-gun, Ibaraki 319-11, Japan
8. Permanent address: Faculty of General Education, Shibaura Institute of Technology, Fukasaku, Ohmiya-shi, Saitama 330, Japan
9. Permanent address: Institute of Space and Astronautical Science, Komaba, Meguro-ku, Tokyo 153, Japan

Abstract

Photoionization of alkali and alkaline-earth atoms has been investigated by means of a time-of-flight mass spectrometer combined with monochromatised synchrotron radiation and an atomic beam, in the wavelength region of 350 - 750 Å. For alkaline-earth atoms, it has been made clear that a two-step autoionization following an innershell excitation plays an important role for doubly charged ions. For alkali atoms, relative photoionization cross sections have been measured for the first time. Moreover, a tentative assignment of spectral lines for Rb and Cs in the complex spectral region has been attemped based on the photoionization data.

1. Introduction

An application of synchrotron radiation in atomic and molecular physics in Japan started with the use of the 750-MeV electron synchrotron at the Institute for Nuclear Study, the University of Tokyo, Tokyo /1/. Several interesting studies, though limited in number, were made with the synchrotron and later with the 400-MeV storage ring (SOR-RING) at the Institute for Solid State Physics, the University of Tokyo, in the same place. Upon the completion of the dedicated synchrotron radiation source (Photon Factory) at Tsukuba /2/, possibilities of extensive research have widely opened.

At the Photon Factory by the end of 1982, eight beam lines were constructed for VUV and soft x-ray experiments. Five beam lines among them are designed mainly for gas-phase experiments. The beam line 11A and 12A are equipped with a grasshopper and Seya-Namioka monochromator, respectively. About ten user groups in the field of atomic and molecular physics have been using those beam lines very actively. The beam lines 12B and 12C are equipped with a 6.65-m off-plane Eagle mounting normal incidence and 10-m grazing incidence monochromator, respectively. These monochromators are used for fairly high resolution spectroscopy of atoms and molecules. The last one is the beam line 2 that provides intense photon flux in the soft x-ray region with the use of an undulator inserted in the storage ring. Detailed descriptions of the Photon Factory, including a 2.5-GeV electron linear accelerator, the 2.5-GeV electron storage ring, beam lines, experimental stations, and users' reports, are given in /3,4,5/.

One of the advantages of making use of the synchrotron radiation is a possibility of studying detailed wavelength dependence of photoabsorption or photoionization in the VUV and soft x-ray region. In the absorption of light in these short-wavelength regions, various innershell processes are expected

to result in rich structures in the spectra. In the present paper, we report such photoionization spectra of alkali (Rb,Cs) and alkaline-earth (Ca,Sr) atoms obtained at the beam line 12A at the Photon Factory. The wavelength ranges covered are: 350 - 420 Å for Ca, 380 - 500 Å for Sr, 420 - 670 Å for Rb, and 640 - 760 Å for Cs. Alkali and alkaline-earth atoms have been chosen because of their simple structure and occupying important positions in the periodic tables, just before the filling of the d-subshell. Also it is interesting to compare their spectra with those of rare gases, for which extensive studies have been already done.

To measure the photoionization spectra, we detected photoions with the use of a time-of-flight (TOF) spectrometer. By using the TOF spectrometer, we can obtain a yield spectrum separately for each stage of ions. This is important because innershell processes often give rise to multiple ionization. The total yield of ions is correctly proportional to the photoionization cross section. This is in contrast with the photographic measurement of photoabsorption, where it is difficult to obtain quantitative information about absorption strength.

The photoion spectroscopy for Ca and Sr was already performed in the above wavelength ranges by Holland and Codling /6/. Their measurements were done with larger wavelength intervals and larger bandpass than ours. The present experiment shows much finer structures in the ion yield spectra, that is, revealing several interesting processes not mentioned in the previous study. Photoion spectra for Rb and Cs have been measured for the first time in the present wavelength ranges.

In the following section (Sec.2), the experimental procedures are described with a brief description about the beam line 12A and the monochromator. Experimental results for Ca and Sr and for Rb and Cs are given

in Secs. 3 and 4, respectively. Section 5 is devoted to mentioning our future experimental schedules.

2. Experimental Method

The beam line and the monochromator are schematically shown in Fig. 1. At the position of 27.28 m from the source point synchrotron radiation with 3 mrad spread in the horizontal direction and 1.5 mrad in the vertical is reflected by a cylindrical SiC mirror M_1, the curvature of which is 1850 mm, to eliminate short wavelength component. Vertical focusing of the incident radiation on the entrance slit of the monochromator is achieved with a platinum-coated concave mirror M_2, the curvature of which is 6250 mm. The synchrotron radiation passing through the slit is dispersed by a gold-coated concave replica grating of 1-m curvature. Monochromatized radiation that passes through the exit slit is focused on a spot of about 1-mmϕ size at the distance of 1200 mm from the center of a refocussing mirrors chamber. The refocussing mirrors consist of two gold-coated plane mirrors and a gold-coated toroidal mirror, the curvature of which is 846 mm on the horizontal direction and 2053 mm in the vertical. Fig. 2 shows the photon flux available when using a 2400 ℓ/mm grating with blazed at 380 Å. The flux has been measured by a sodium salicylate screen plus photomultiplier combination and normalized to the absolute values, which were determined by using a double-ion chamber, at several points.

A schematic drawing of the TOF mass spectrometer and a furnace for atomic beam is shown in Fig. 3. The atomic vapour was produced in the resistively heated furnace and effused from the orifice of it, which was located 5 cm beneath the collision region. The photon beam crosses the atomic beam at right angles. An electrostatic deflector and a collimating aperture

were placed between the furnace orifice and the collision region. The deflector electrode removes thermal ions from the furnace when heated up.

The TOF mass spectrometer consisted of three sections, namely, an ionization section, an acceleration section, and a field-free drift section. The length of the last section is 44 cm. This long drift tube was adopted to protect an ion detector from contamination of metal vapour. The spectrometer was operated under double-field space focusing conditions /7/. A voltage pulse of height +100 V and width about 4 μsec was applied to an ion-repeller electrode in order to push photoions to the drift tube, whose axis is perpendicular to both the atomic and photon beams. At the same time, a time-to-amplitude converter (TAC) was triggered by the pulse. After accelerated further between a front cap and the drift tube, the photoions entered the drift section and were finally detected by the ion detector, tandem microchannel plate (MCP). The output signal of the MCP was used as a stop pulse of the TAC. The intensity ratio of the doubly charged photoions and the singly charged photoions was examined against the negative voltage applied to the input surface of the MCP, and the ratio was assured to be almost constant provided that the voltage exceeded -4 kV.

A TOF spectrum can be obtained also in another mode which correlates the detection of photoelectrons accelerated in the opposite direction to that of photoions. In this method, the TAC was triggered by an output pulse of the electron detector, channeltron. Since this method has a much higher detection-efficiency for doubly charged ions than for singly charged ions, it cannot be relied upon in obtaining the ratio data. However, this method served to corroborate the qualitative features of the intensity ratio.

The block diagram of a data acquisition and control system is shown in Fig. 4. As mentioned above, the timing signal of the pulse generator started

the TAC and the output signal of the photoion detector stopped the TAC. The output signals of the TAC, which correspond to the flight-times of the photoions, were stored with a pulse-height analyzer (PHA). The typical TOF spectra of Sr recorded at wavelengths of 498 and 405 Å are shown in Fig. 5. To obtain the ion-yield spectrum for each stage of ions, gates on the TAC's were set such that the TAC's gave output pulses corresponding to singly charged ions, doubly charged ions or background. Counts in these three channels were then registered to a computer at every wavelength intervals, and normalized to the photon flux monitored by a sodium salicylate screen plus photomultiplier combination.

3. Single and Double Photoionization of Alkaline-earth Atoms (Ca,Sr)

Relative cross sections, q^+ and q^{++}, each for single and double photoionization have been measured in the regions below and above Ca 3p- and Sr 4p-subshell ionization /8,9/. For these atoms, the photoabsorption measurements using a photographic technique have been reported by Mansfied and Newsom /10,11/ and these were very useful in identifying the peak structure in our ion-yield spectra. However, their absorption spectra may suffer from saturation and can not be relied on to derive the strength of photoabsorption. The present ion-yield spectra in /8,9/ could be useful as the standards of the relative photoionization cross sections. Moreover, by separately measuring q^+ and q^{++}, useful information has been obtained on the ionic final states after excitation.

The Ca^+ and Ca^{++} ion-yield spectra measured with a bandwidth of 1.5 Å are shown in Figs. 6(a) and (b). We can see a good correspondence between the peak structures in the Ca^+ and Ca^{++} spectra. The most prominent peak appears at 394.8 Å (31.40 eV) in both the Ca^+ and Ca^{++} spectra. This peak corresponds

to the $3p^6 4s^2\ ^1S_0 \rightarrow 3p^5 3d4s^2\ ^1P_i$ dipole resonance observed in the photoabsorption measurement /10/. Four series (ns and nd) converging to the $3p^5 4s^2\ ^2P_{3/2}$ limit at 361.3 Å (34.32 eV) and to the $3p^5 4s^2\ ^2P_{1/2}$ limit at 357.7 Å (34.66 eV) are indicated in Fig. 6. Our assignment is based on the photoabsorption spectrum of Mansfield and Newsom /10/. The autoionizing states formed by these single-electron excitations constitute dominant peak structures in the ion-yield spectra for the energies below the $3p^5 4s^2\ ^2P_{3/2,1/2}$ limits. In addition to these lines, there also appear a number of supernumerary lines which must be caused by multi-electron excitations arising through configuration mixing. Above the $3p^5 4s^2\ ^2P_{3/2,1/2}$ limits, the Ca^+ yield falls to a quite low level while the Ca^{++} yield grows, because a singly charged ion with an inner-shell hole predominantly decays via the Auger transition to a doubly charged ion.

We have proposed in /8/ that, below the $3p^5 4s^2\ ^2P_{3/2,1/2}$ limits, the following two-step autoionization plays an important role in the Ca^{++} production. Namely, photoexcited states $Ca^*(\cdots 3p^5 4s^2\ n\ell)$ autoionize to intermediate states, such as $Ca^{+*}(\cdots 3p^5 3d4s\ ^4P$ and $(^3P)^2P)$:

$$Ca^*(\cdots 3p^5 4s^2\ n\ell) \rightarrow Ca^{+*}(\cdots 3p^5 3d4s\ ^4P \text{ and } (^3P)^2P) + e_1 \ . \qquad (1)$$

These intermediate states subsequently autoionize to the ground state of Ca^{++} as

$$Ca^{+*}(\cdots 3p^5 3d4s\ ^4P \text{ and } (^3P)^2P) \rightarrow Ca^{++}(\cdots 3p^6\ ^1S) + e_2 \ , \qquad (2)$$

31.08 eV	31.58 eV	17.99 eV
30.99	31.47	
30.92		

where the numbers written beneath the term symbols indicate the state energies

measured from the ground state of Ca. This two-step autoionization mechanism is supported by the photoelectron data of Bizau et al. /12,13/, however, they do not explicitly refer to the two-step autoionization in their papers. Because the energies of the intermediate states for the two-step autoionization have been well established by Mansfield and Ottely /14/ (although Bizau et al. /13/ mentioned that they measured the lowest 3p-ionization threshold, at 30.8 eV, for the first time, their description is not correct!), the energies of the electrons e_1 and e_2 in Eqs. (1) and (2) can be determined automatically. The electron e_2 having the energy of 13.0 eV originates from the ^4P states, while the electron e_2 of 13.6 eV comes from the ^2P states. These autoionization peaks were observed by Bizau et al. at the photon energies 31.62 eV /12/ and 31.99 eV /13/. The former energy corresponds to the higher energy tail of $Ca^*(\cdots 3p^5 3d4s^2\ ^1P_1)$ excitation peak and the latter correspond to $Ca^*(\cdots 3p^5 4s^2\ ^2P_{3/2}\ 5s)$. Comparing those two spectra, an energy shift of the peak around 13.6 eV is clearly seen due to post-collision interaction effects caused by the slow e_1 electrons; at the photon energy 31.62 eV the energy of e_1 is only about 0.095 eV.

Pejcev et al. /15/ and Schmitz et al. /16/ found the leading 3p ionization limits, $3p^5 4s^2\ ^2P_{1/2}$, $^2P_{3/2}$ and $3p^5 3d(^3P)4s\ ^2P$, in the ejected electron spectra induced by electron impact. On the consideration that the two-step autoionization occurs via these intermediate states, their results are consistent with our finding that the intensity ratio of Ca^{++} to Ca^+ shows a step-like increase at these ionization limits /8/.

The Sr^+ and Sr^{++} ion-yield spectra measured with a bandwidth of 0.8 Å are shown in Figs. 7(a) and (b). The general features of these spectra bear a strong resemblance to those seen previously in Ca. The main series whose members we have been able to identify are shown in Fig. 7. This assignment is

based on the photoabsorption data by Mansfield and Newsom /11/. The Rydberg series $4p^5 5s^2(^2P_{1/2})nd$ and its associated continum $4p^5 5s^2\,(^2P_{1/2})\varepsilon d$ are predominant in these spectra. The 4d and 5d members of this series are apparent in the Sr^+ ion yield spectrum, though, the 4d member, corresponding to the strongest resonance line at 491 Å, is not shown in Fig. 7 due to the limit of the space. The higher members 6d to 9d, as well as the 5d, can be seen between 430 and 440 Å in the Sr^{++} ion-yield spectrum and are indicated by arrows.

As in the case of Ca, a two-step autoionization plays an important role above the lowest 4p ionization limit $4p^5 4d5s^2\ ^4P_{1/2}$. From the ejected electron spectra taken by White et al. /17/ and Schmitz et al. /16/ using the electron impact method, the ionization limits, $4p^5 5s^2\ ^2P_{1/2}$, $4p^5 5s^2\ ^2P_{3/2}$, and $4p^5 4d(^3P)5s\ ^2P_{3/2}$, are considered important as the intermediate states for the two-step autoionization. Actually an increase in the Sr^{++} ion intensity is seen at these three ionization limits. Between the $4p^5 5s^2\ ^2P_{1/2}$ and $^2P_{3/2}$ limits, main features corresponding to the above mentioned states from 6d to 9d show asymmentric autoionization-profiles. The asymmetric Beutler-Fano profiles are caused by interference between the direct photoionization channel to the $4p^5 5s^2\ ^2P_{3/2}$ limit and the autoionization channel such as

$$Sr^*(\cdots 4p^5 5s^2(^2P_{1/2})nd) \rightarrow Sr^{+*}(\cdots 4^5 5s^2\ ^2P_{3/2}) + e_1 \ . \qquad (3)$$

The asymmetric profiles are seen in the Sr^{++} ion yield spectrum, as the $4p^5 5s^2\ ^2P_{1/2}$ state autoionizes to the ground state of Sr^{++}. This fact, i.e. the interference profiles seen in the Sr^{++} spectrum, must be one evidence of the existence of the two-step autoionization decay. However, to examine the two-step autoionization directly, a further study is needed of photoelectron spectroscopy in the energy region of the 4p excitation.

The photoionization spectra of the subvalence np-subshells of Sr(n=4) and Ca(n=3) are very similar in many respects. However, there is one big difference between them; in the Sr case the $4p^5 5s^2(^2P_{1/2})4d$ state leading to giant the 4p → 4d resonance peak at 491 Å lies fairly below the lowest 4p ionization limit, making the two-step autoionization energetically impossible. Nevertheless, our ion-yield spectra show a non-negligible Sr^{++} component in the region of the resonance. In order to examine this phenomenon in more detail, TOF mass spectra with long accumulation time around this peak were measured. They indicate that Sr^{++} ions are produced only at the resonance position; the yield of Sr^{++} ions amounts to about 2 % of that of Sr^+. These Sr^{++} ions are probably produced by a double-Auger process; the resonance state $4p^5 5s^2(^2P_{1/2})4d$ decays to the ground state of Sr^{++} by emitting two electrons simultaneously.

4. Photoionization of Alkali Atoms (Rb, Cs)

Yield spectra of singly charged ions of Rb and Cs have been measured in the energy regions below the double-ionization thresholds, 31.47 and 32,28 eV (394.0 and 384.1 Å) for Rb and 27.06 and 28.78 eV (458.2 and 430,8 Å) for Cs. As the excited states of the np-subshell electrons of Rb(n=4) and Cs(n=5) are located much above the single-ionization thresholds, 4.177 eV (2968 Å) for Rb and 3.894 eV (3184 Å) for Cs, the excitations of those electrons mostly result in autoionization. For this reason, the present ion-yield spectra are almost identical to the relevant photoabsorption spectra except for the quartet states, which are forbidden for autoionization. In contrast to the photoabsorption spectra obtained with a photographic method, the ion-yield spectra give the quantitative information on the photoabsorption intensities.

The ion-yield spectrum of Rb measured with a bandpass of 0.4 Å is shown

in Fig. 8. In this energy region, there are several photoabsorption spectroscopic studies /18,19,20,21/, but, so far as we know, all of the lines have not been definitely assigned. Six 4p-ionization limits determined by Reader and Epstein /22/ are indicated on the top of the spectrum. A tentative assignment has been attempted, based quantum-defect comparisons and intensity distributions of relevant lines. Between the $4p^5(^2P_{1/2})5s$ and $4p^5(^2P_{3/2})5s$ limits asymmetric Beutler-Fano autoionization profiles can be seen but are not so clear as those seen in the Sr case. Also the structures between these series limits are largely different from the autoionization structures observed in Kr between its $^2P_{1/2}$ and $^2P_{3/2}$ ionic states /23/. Detailed analysis of the photoionization spectrum is in progress.

The ion yield spectrum of Cs measured with a bandpass of 0.4 Å is shown in Fig. 9. Rydberg series approaching to the four 4p ionization limits, which are prominent in the photoelectron spectrum by Süzer et al. /24/, are indicated on the top of the spectrum. The Rydberg series $5p^56sns$ and $5p^56snd$ converging to the limits $(^2P_{1/2})6s$, J=0,1 are clearly seen between the $5p^5(^2P_{3/2})6s$ and $5p^5(^2P_{1/2})6s$ limits, as observed in the photoabsorption spectrum of Kaufmann et al. /25/. Unlike the photoabsorption spectrum which suffers from saturation, the present ion yield spectrum gives the relative photoionization cross section which provides quantitative information for the asymmetric Beutler-Fano autoionization profiles. In contrast to Rb, the Cs spectrum has a very similar structure to the autoionization structures observed in Xe between its $^2P_{3/2}$ and $^2P_{1/2}$ ionic states /23/.

Below both limits $(^2P_{3/2})6s$, J=1,2, a tentative assignment has been attempted on the basis of quantum-defect comparisons and intensity distributions of relevant lines /27/. The result is shown in Fig. 9 and serves as a revision of the works of Beutler and Guggenheimer /28/ and Connerade /29/. To

confirm the present assignment, accurate theoretical calculations of the term energies are needed.

5. Future Problems

The present program of atomic photoionization will be extended to higher photon-energy regions, that is, to the regions for excitations of deeper shells than the subvalence p-subshells, using the grasshopper monochromator. As the production of multiply charged ions is expected to occur via Auger cascade decays, the decay channels of innershell excited-states will be much complicated compared to the present case. Therefore, photoelectron spectroscopy will be required to study such a complicated decay mechanism.

In the case of Rb and Cs, a surface ionization detector can be used to monitor intensities of those atomic beams. So our second plan is absolute measurements of the photoionization cross section for the alkali atoms. It is important to compare experimental cross sections with theoretical ones (for example, we can cite the work of Hung and Starace for Cs /30/) in absolute scale to examine the validity of theories.

Acknowledgements

The authors are grateful to Professors T. Sasaki and B. Sonntag and Doctor J.B. West for their participation in the some parts of this program. They thank to the staff of the Photon Factory for providing facilities and much photons.

This work was supported in part by the Japan Society for the Promotion of Science under a Japan-USA Cooperative Research Program.

This work was performed under the approval of the Photon Factory Program Advisory Committee (Proposal No. 84-029).

References

1. Nakamura M., Sasanuma M., Sato S., Watanabe M., Yamashita H., Iguchi Y., Ejiri A., Nakai S., Yamaguchi S., Sagawa T., Nakai Y. and Oshio T.: Phys. Rev. 178, 80 (1969)
2. Kohra K. and Sasaki T.: Nucl. Instrum. Meth. 208, 23 (1983)
3. Photon Factory Activity Report 1982/83, Tsukuba, National Laboratory for High Energy Physics, 1984
4. Photon Factory Activity Report 1983/84, Tsukuba, National Laboratory for High Energy Physics, 1985
5. Photon Factory Activity Report 1984/85, Tsukuba, National Laboratory for High Energy Physics, 1986
6. Holland D.M.P. and Codling K.: J. Phys. B 14, 2345 (1981)
7. Wiely W.C. and McLaren I.H.: Rev. Sci. Instrum. 26, 1150 (1955)
8. Sato Y., Hayaishi T., Itikawa Y., Itoh Y., Murakami J., Nagata T., Sasaki T., Sonntag B., Yagishita A., and Yoshino M.: J. Phys. B 18, 225 (1985)
9. Nagata T., West J.B., Hayaishi T., Itikawa Y., Itoh Y., Koizumi T., Murakami J., Sato Y., Shibata H., Yagishita A., and Yoshino M.: J. Phys. B 19, 1281 (1986)
10. Mansfield M.W.D. and Newsom G.H.: Proc. R. Soc. Lond. A 357, 77 (1977)
11. Mansfield M.W.D. and Newsom G.H.: Proc. R. Soc. Lond. A 377, 431 (1981)
12. Bizau J.M., Wuilleumier F.J., G. Wedin, and Dhez P.: Int. Conf. on X-ray and Atomic Inner-Shell Physics, Eugene, Oregon, Abstract p.151 (1982)
13. Bizau J.M., Gêrard P., Wuilleumier F.J., and Wedin G.: Phys. Rev. Lett, 53 2083 (1984)
14. Mansfield M.W.D. and Ottley T.W.: Proc. R. Soc. Lond. A 365, 413 (1979)
15. Pejcev V., Ottley T.W., Rassi D., and Ross K.J.: J. Phys. B 11, 531 (1978)

16. Schmitz W., Breuckmann B., and Mehlhorn W.: J. Phys. B 16, L492 (1976)
17. White M.D., Rassi D., and Ross K.J.: J. Phys. B 12, 315 (1979)
18. Beutler H.: Zs. f. Phys., 91, 132 (1934)
19. Connerade J.P.: Astrophys. J., 159, 695 (1970)
20. Mansfield M.W.D.: Astrophys. J., 183, 691 (1973)
21. Mansfield M.W.D.: Proc. R. Soc. Lond., A 364, 135 (1978)
22. Reader J. and Epstein G: J. Opt. Soc. Am., 63, 1153 (1973)
23. Huffman R.E., Tanaka Y., and Larrabee J.C.: J. Chem. Phys., 39 902 (1963)
24. Süzer S., Breuchmann B., Menzel W., Theodosiou C.E., and Mehlhorn W.: J. Phys. B 13, 2061 (1980)
25. Kaufman V., Sugar J., Clark C.W., and Hill III W.T.: Phys. Rev. A 28, 2876 (1983)
26. Reader J.: Phys. Rev. A 13, 507 (1976)
27. Yoshino M., Hayaishi T., Itikawa Y., Itoh Y., Koizumi T., Nagata T., Sato Y., Shibata H., and Yagishita A.: to be published in J. Phys. B
28. Beutler H. and Guggenheimer K.: Zs. f. Phys., 88, 25 (1934)
29. Connerade J.P: Astrophys. J., 159, 685 (1970)
30. Huang K.-H and Starace A.J.: Phys. Rev., A 22, 318 (1980)

Figure captions

Fig. 1. Schematic drawing of the beam line 12A and the Seya-Namioka monochromator. The height of monochromatized radiation is 1350 mm from the 2nd floor.

Fig. 2. Photon flux for 400 μm - 400 μm slit widths and 150 mA ring current.

Fig. 3. Schematic drawing of the TOF mass spectrometer and the metal-atom beam source.

Fig. 4. Block diagram of a data acquisition and control system for taking TOF spectra and ion-yield spectra.

Fig. 5. Typical TOF spectra of Sr. At the wavelength 498 Å, longer wavelength than 491 Å for the 4p→4d giant resonance peak, the signals of Sr^{++} ions are not seen. We can see the O_2^+ and O^+ peaks of residual gas components, because these spectra were measured under not so good background pressure.

Fig. 6. (a) Ca^+ and (b) Ca^{++} yield spectra. The $3p^5 4s^2 nd,ns$ Rydberg series converging to the $3p^5 4s^2\ ^2P_{1/2,3/2}$ limits are indicated, together with the Ca^+ $3p^5 3d4s\ ^4P$ and Ca $3p^5(3d^3\ ^2P)^3P_1$ states.

Fig. 7. (a) Sr^{++} and (b) Sr^+ yield spectra. Arrows indicate the 5d to 9d members of the $4p^5 5s^2(^2P_{1/2})nd$ series, of which 6d to 9d show asymmetric Beutler-Fano autoionization profiles.

Fig. 8. Rb^+ yield spectrum. The 4p ionization limits determined by Reader and Eqstein /22/ are indicated.

Fig. 9. Cs^+ yield spectrum. The 5p ionization limits determined by Reader /26/ are used to identify this spectrum.

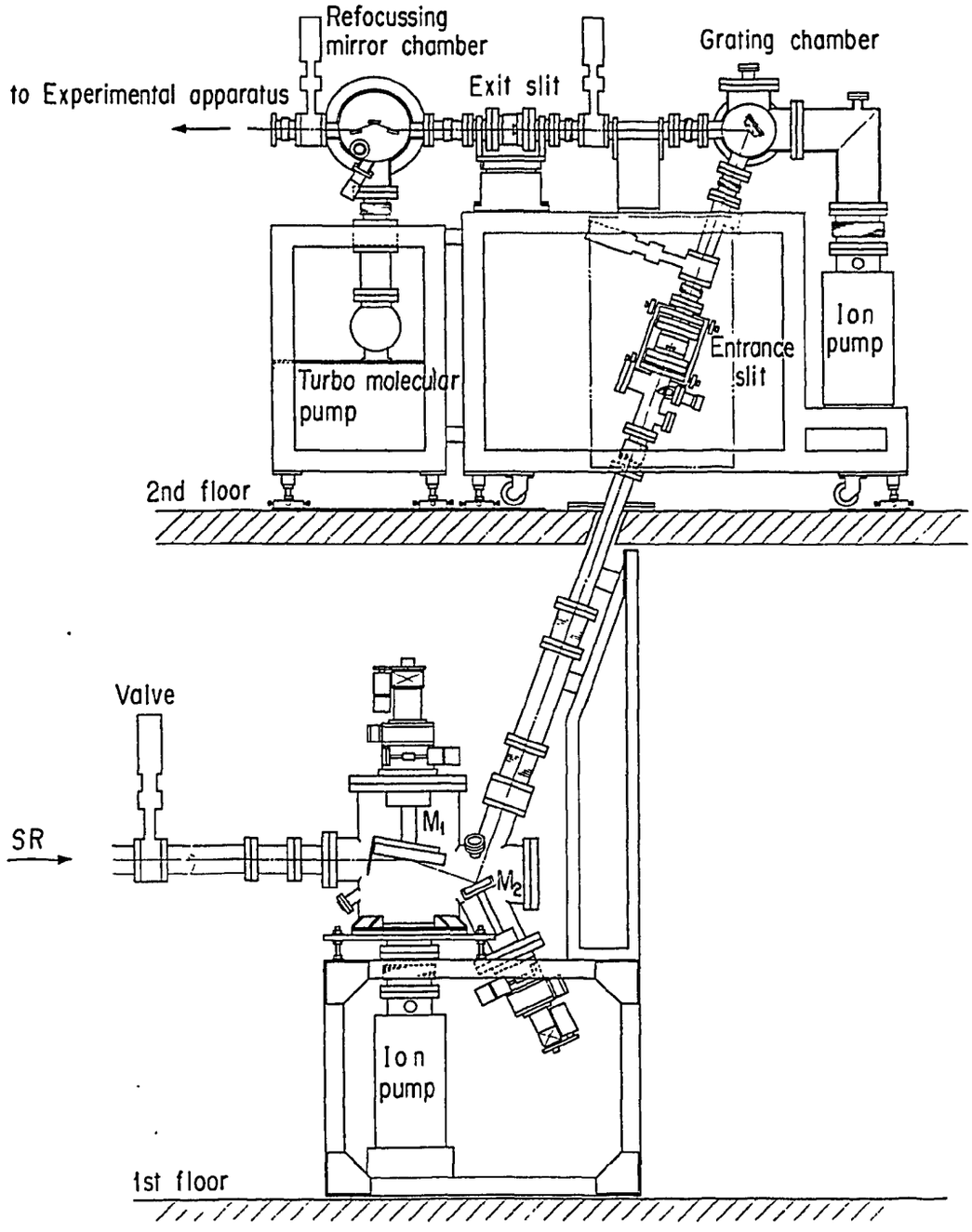
Refocussing
mirror chamber
Grating chamber
to Experimental apparatus
Exit slit
Ion
pump
Entrance
slit
Turbo molecular
pump
2nd floor
Valve
SR
M1
M2
Ion
pump
1st floor

Fig. 1

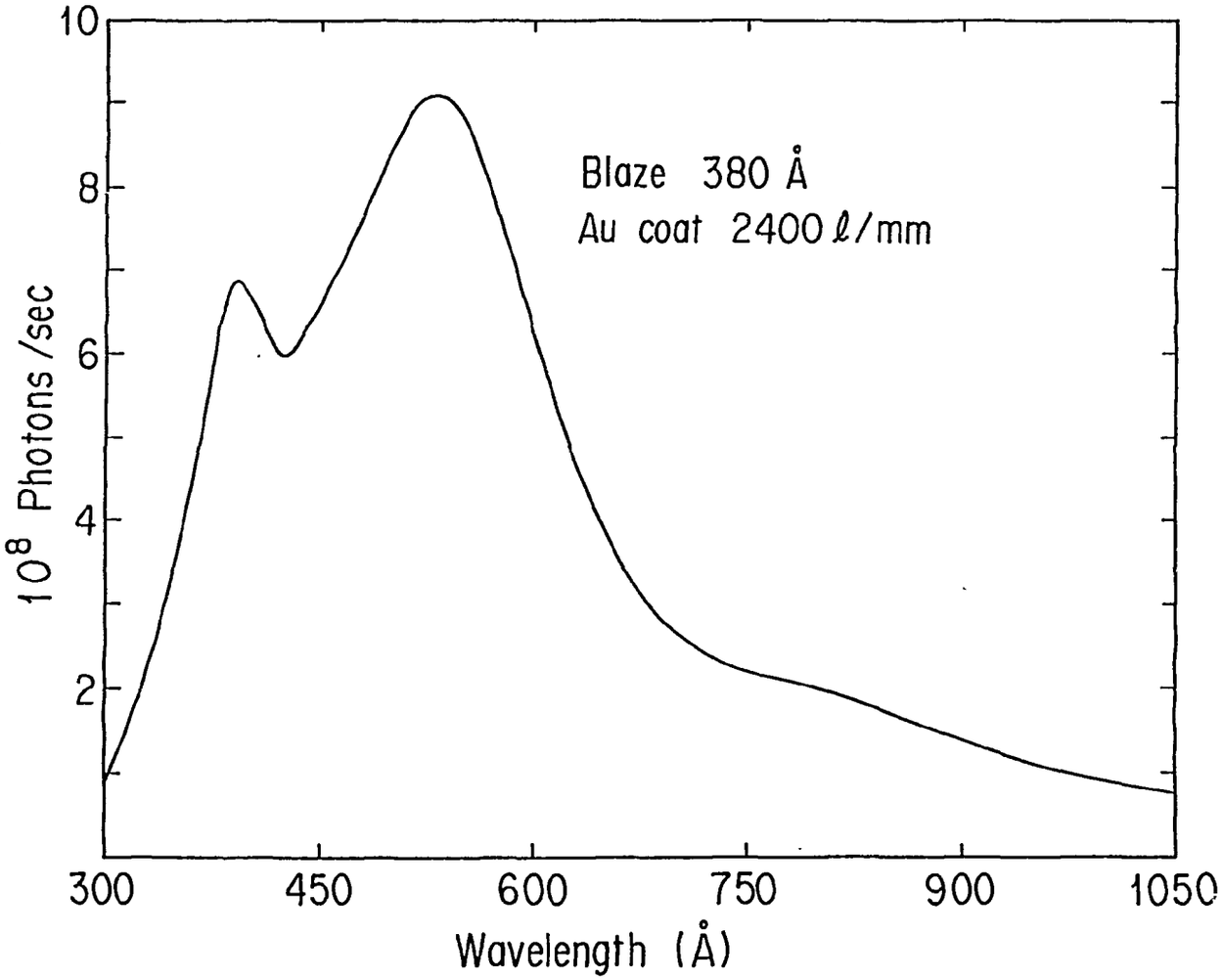
10
8
6
4
2
10^8 Photons /sec
Blaze 380 Å
Au coat 2400 ℓ/mm
300
450
600
750
900
1050
Wavelength (Å)

Fig. 2

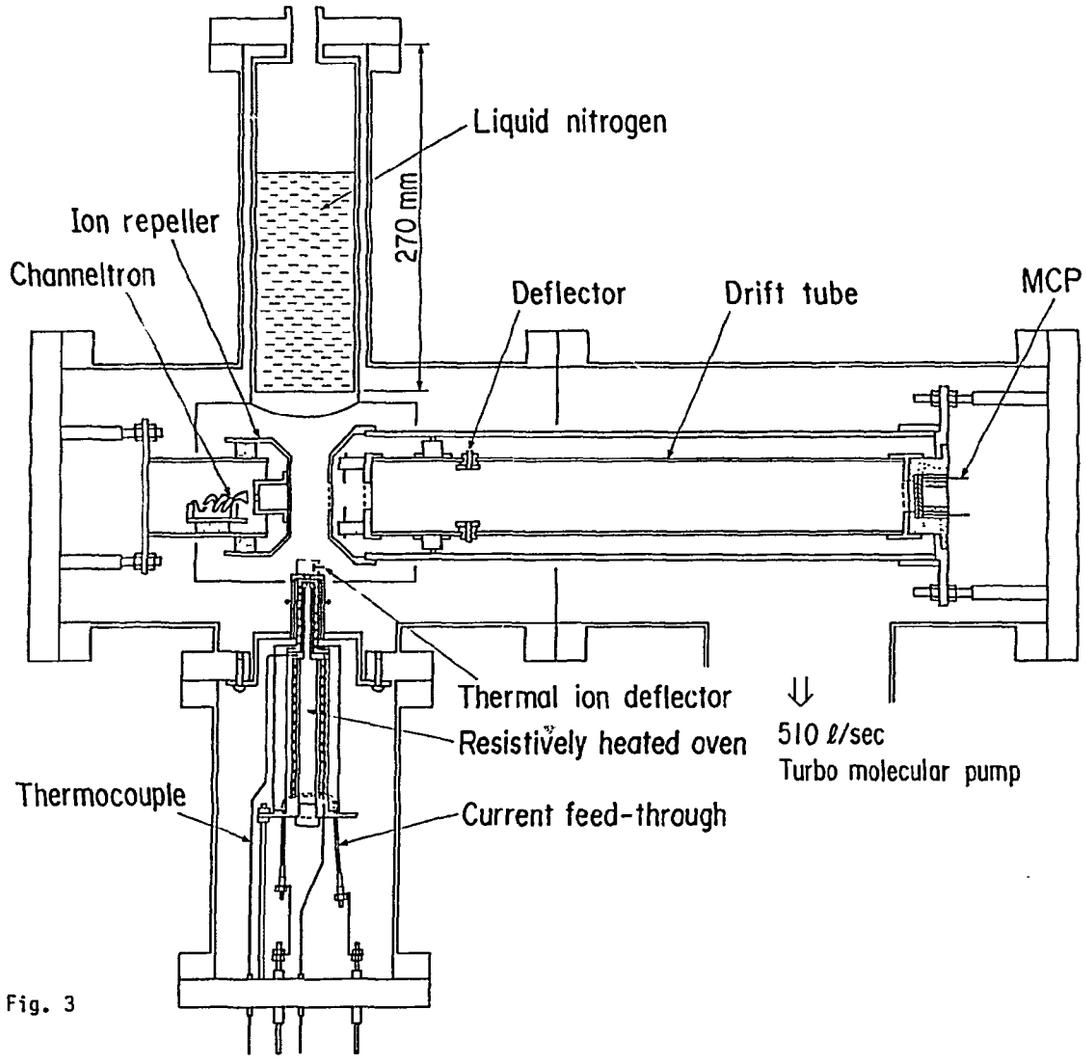
Liquid nitrogen
270 mm
Ion repeller
Channeltron
Deflector
Drift tube
MCP
Thermal ion deflector
Resistively heated oven
510 ℓ/sec
Turbo molecular pump
Thermocouple
Current feed-through

Fig. 3

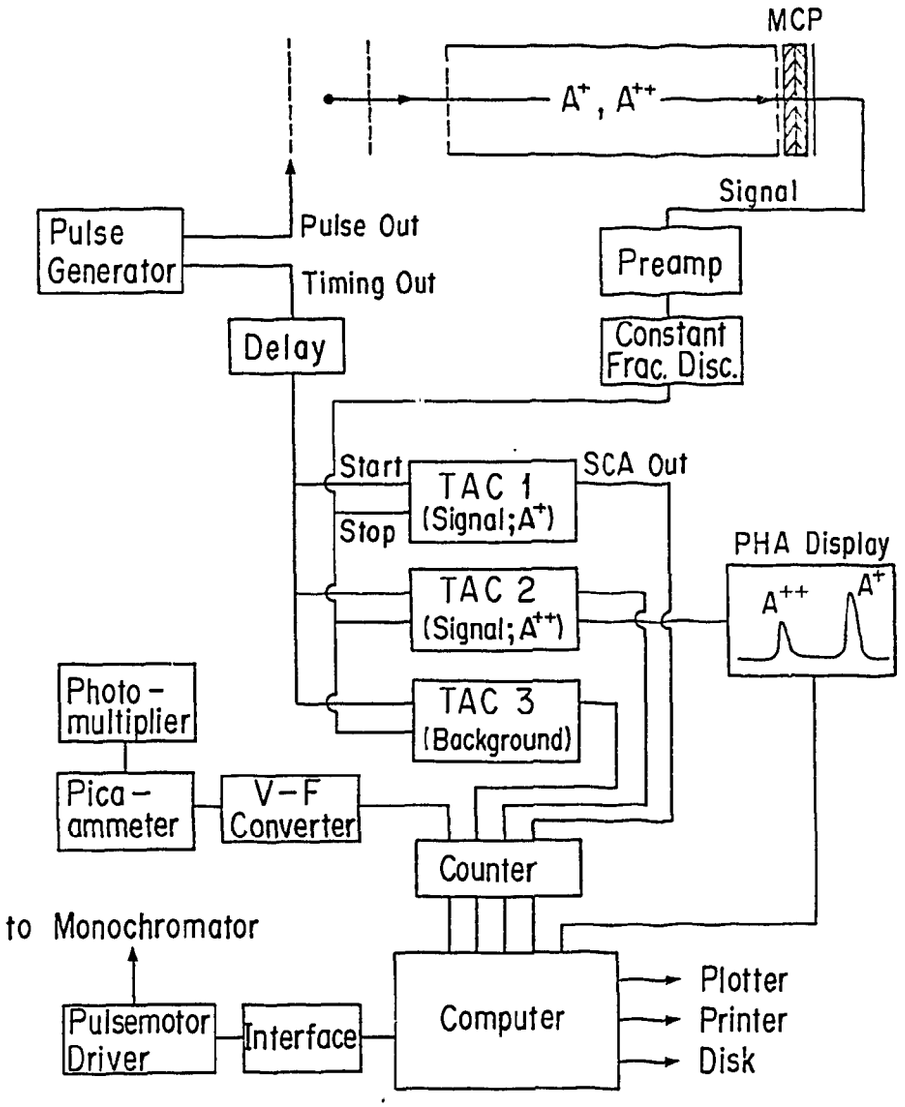
MCP
A+, A++
Signal
Pulse Generator
Pulse Out
Timing Out
Preamp
Delay
Constant Frac. Disc.
Start
Stop
TAC 1 (Signal;A+)
SCA Out
PHA Display
A++
A+
TAC 2 (Signal;A++)
Photo-multiplier
TAC 3 (Background)
Pica-ammeter
V-F Converter
Counter
to Monochromator
Pulsemotor Driver
Interface
Computer
Plotter
Printer
Disk

Fig. 4

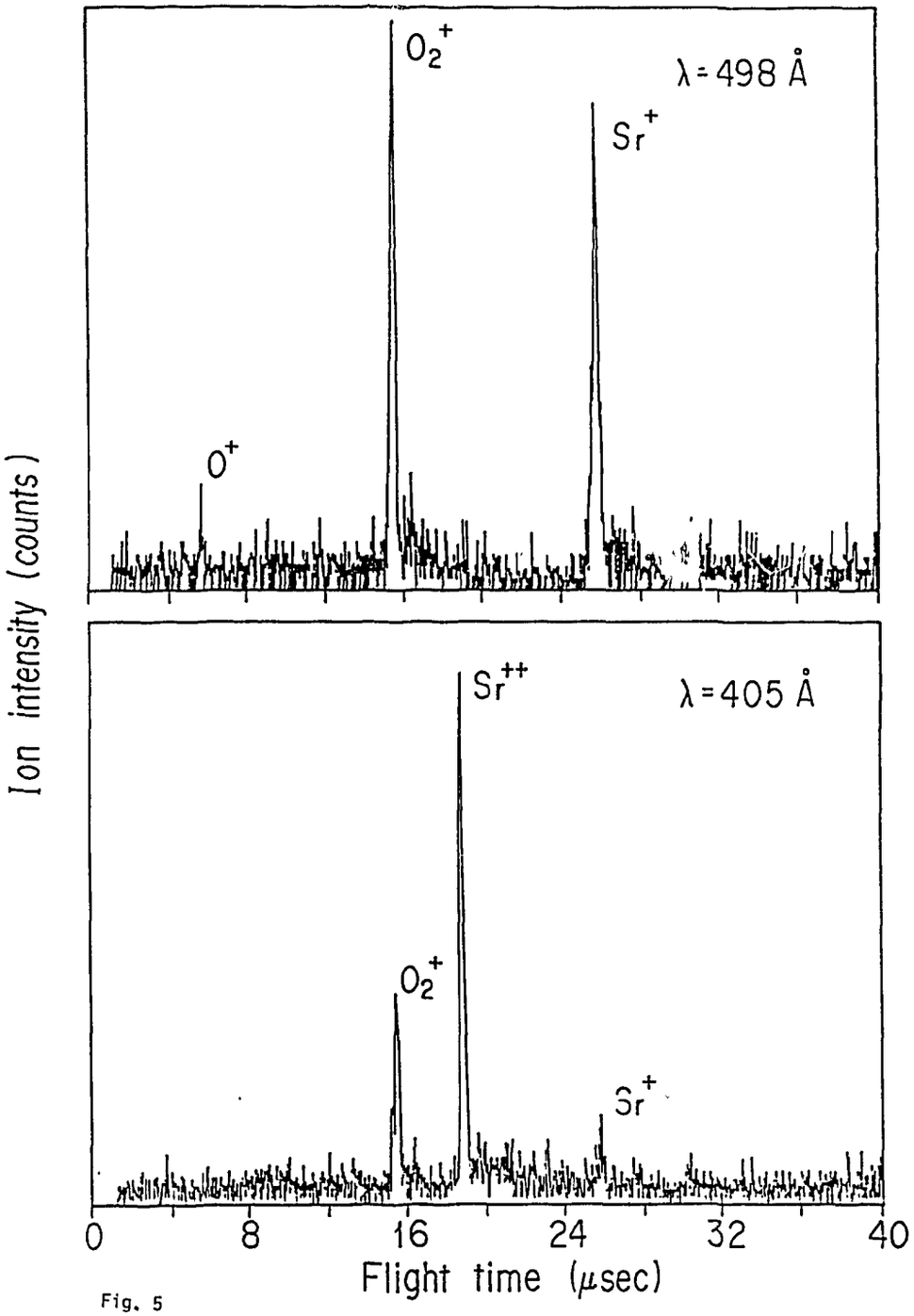
O_2^+
λ = 498 Å
Sr^+
O^+
Sr^{++}
λ = 405 Å
O_2^+
Sr^+
Ion intensity (counts)
0
8
16
24
32
40
Flight time (μsec)

Fig. 5

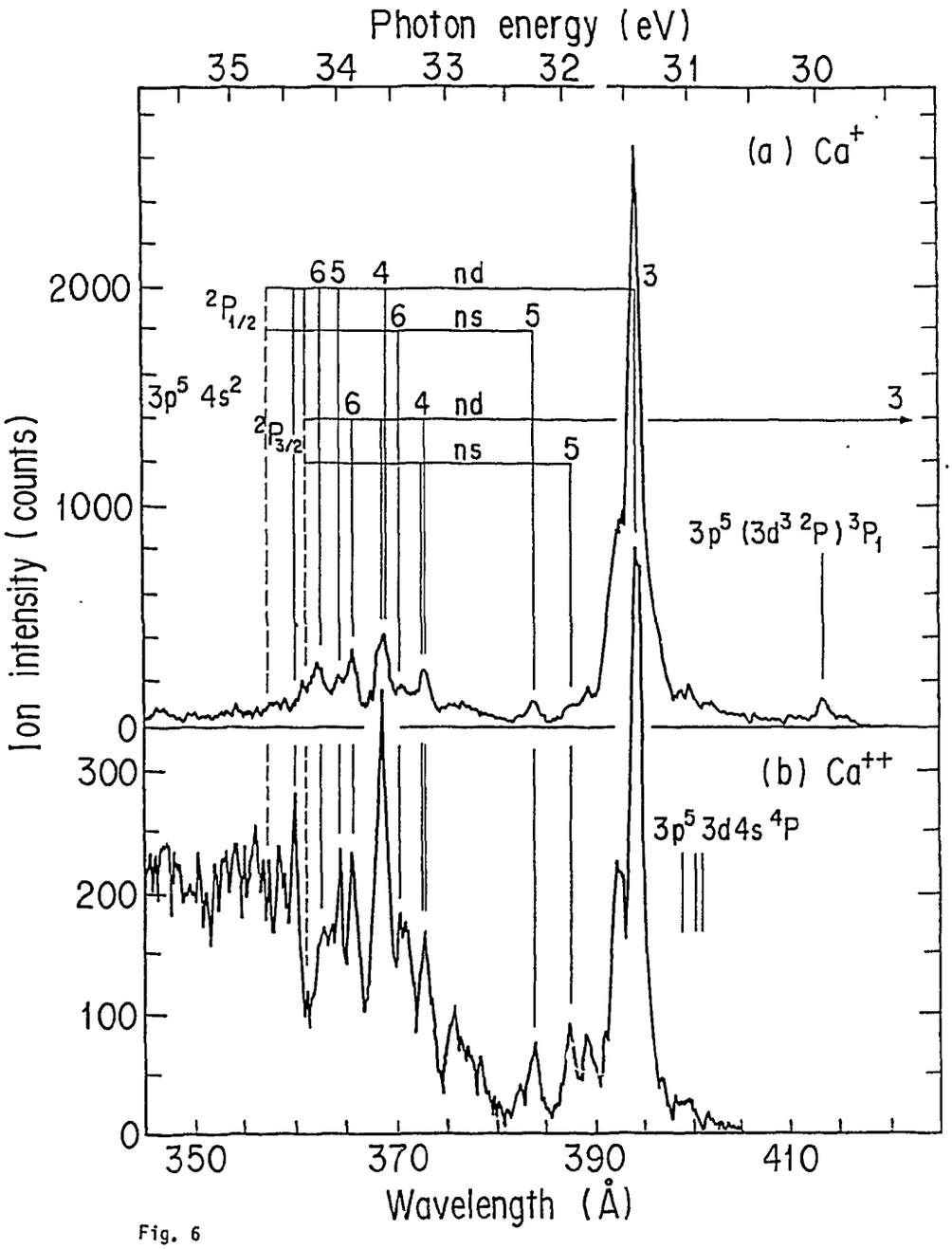
Photon energy (eV)
35
34
33
32
31
30
(a) Ca+
2000
1000
0
65 4 nd
3
2P1/2
6 ns 5
3p5 4s2
6 4 nd
3
2P3/2
ns 5
3p5 (3d3 2P) 3P1
Ion intensity (counts)
(b) Ca++
300
200
100
0
3p5 3d4s 4P
350
370
390
410
Wavelength (Å)

Fig. 6

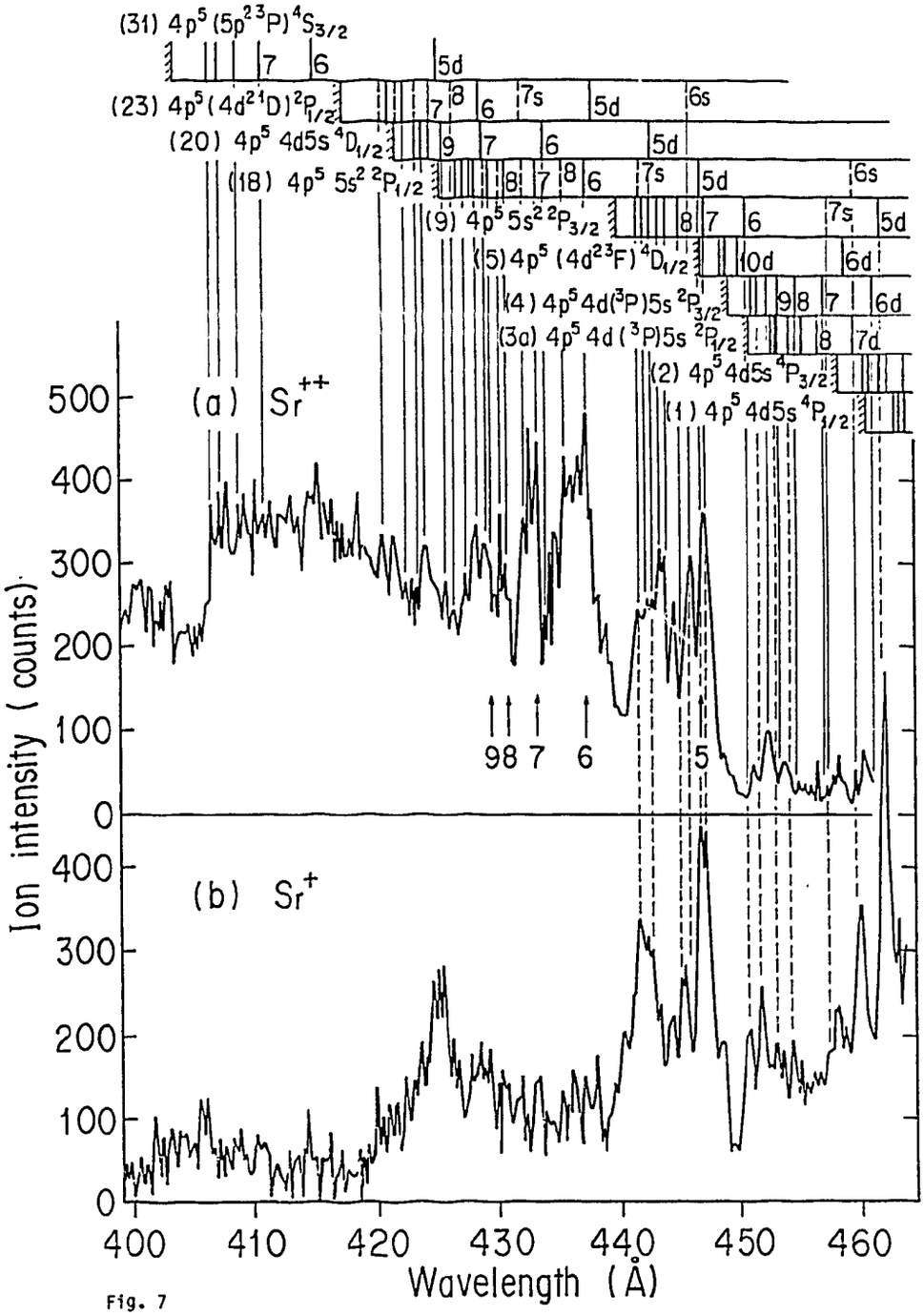
(31) 4p5 (5p2 3P) 4S3/2
(23) 4p5 (4d2 1D) 2P1/2
(20) 4p5 4d5s 4D1/2
(18) 4p5 5s2 2P1/2
(9) 4p5 5s2 2P3/2
(5) 4p5 (4d2 3F) 4D1/2
(4) 4p5 4d(3P)5s 2P3/2
(3a) 4p5 4d (3P)5s 2P1/2
(2) 4p5 4d5s 4P3/2
(1) 4p5 4d5s 4P1/2
(a) Sr++
(b) Sr+
9 8 7 6
5
Ion intensity (counts)
Wavelength (Å)
0
100
200
300
400
500
400
410
420
430
440
450
460

Fig. 7

Fig. 9

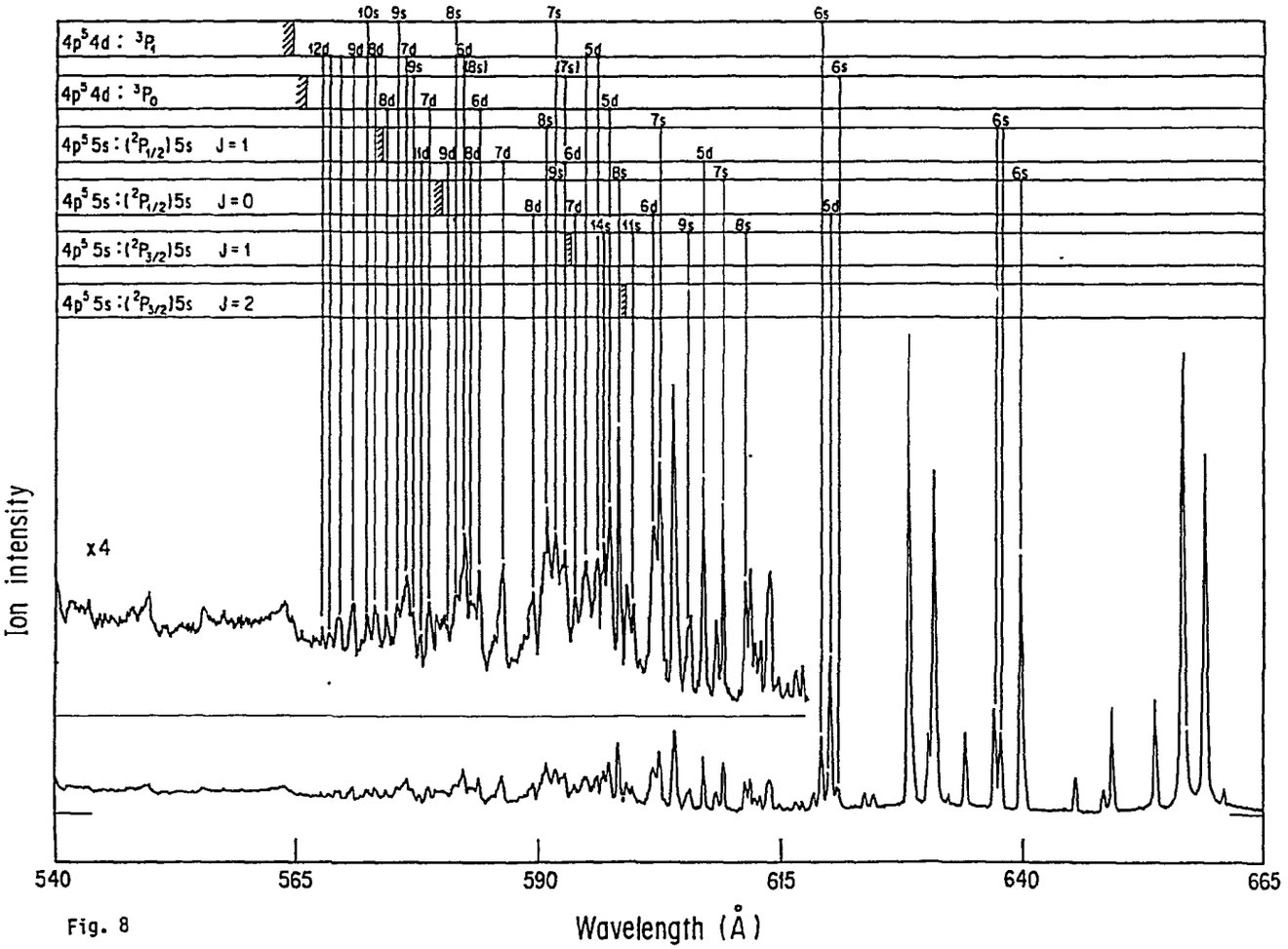
Wavelength (A)
4p⁵4d : ³P₁
4p⁵4d : ³P₀
4p⁵5s : (²P₁/₂)5s J = 1
4p⁵5s : (²P₁/₂)5s J = 0
4p⁵5s : (²P₃/₂)5s J = 1
4p⁵5s : (²P₃/₂)5s J = 2
x4
Ion intensity
540
565
590
615
640
665
Wavelength (Å)

Fig. 8

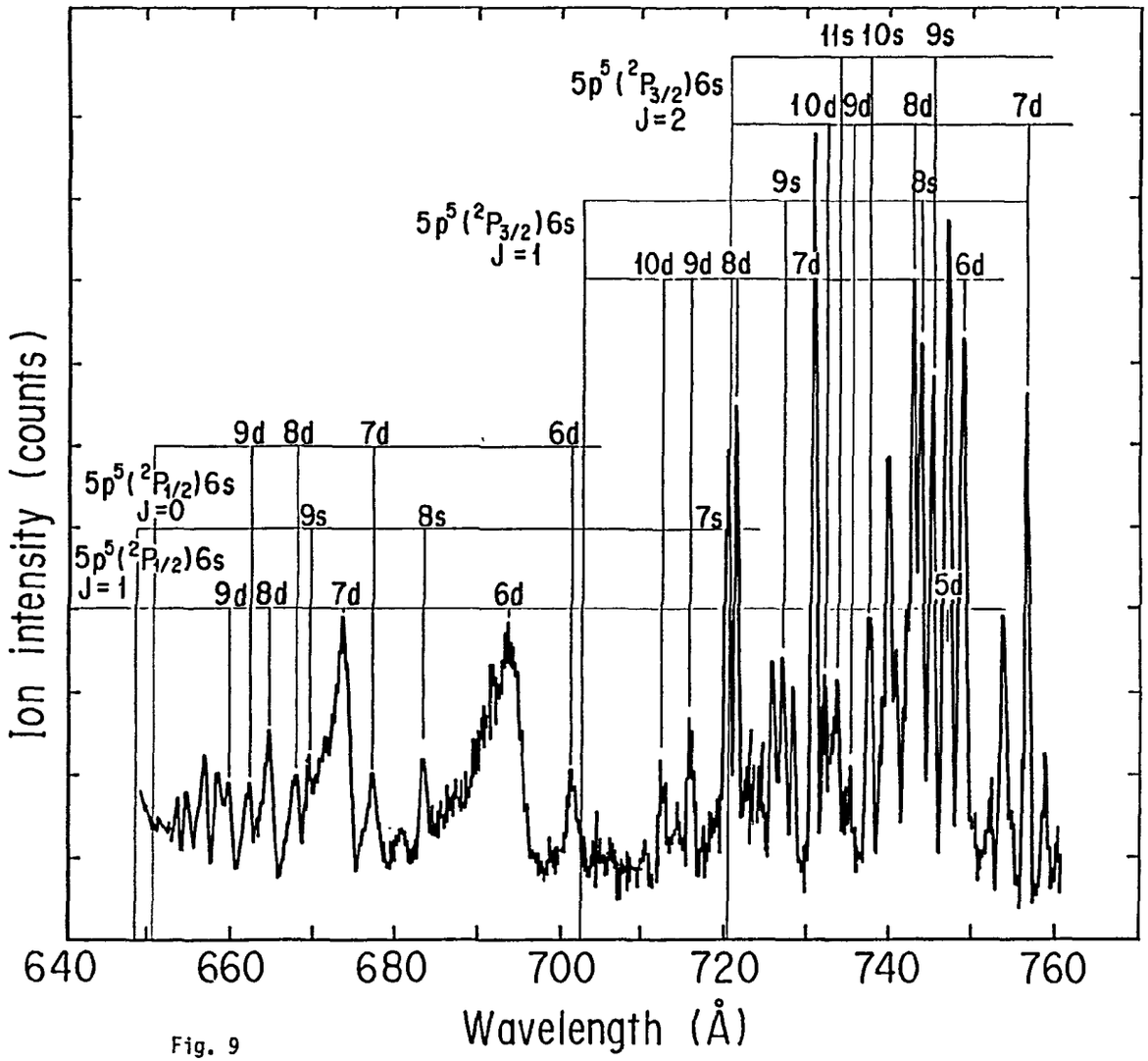
11s 10s 9s
$5p^5(^2P_{3/2})6s$
J=2
10d 9d 8d 7d
9s 8s
$5p^5(^2P_{3/2})6s$
J=1
10d 9d 8d 7d 6d
9d 8d 7d 6d
$5p^5(^2P_{1/2})6s$
J=0
9s 8s 7s
$5p^5(^2P_{1/2})6s$
J=1
9d 8d 7d 6d 5d
Ion intensity (counts)
640 660 680 700 720 740 760
Wavelength (Å)

Fig. 9